AIAA JOURNAL
Vol. 42, No. 10, October 2004

Assessment of Equation Solvers and Optimization Techniques for Nonaxisymmetric Liners

W. R. Watson,* M. G. Jones,† T. L. Parrott,‡ and J. Sobieski§
NASA Langley Research Center, Hampton, Virginia 23681-2199

CPU times and memory requirements for a commonly used solver are compared to that of a state-of-the-art, parallel, sparse solver. The sparse solver is then used in conjunction with three optimization methodologies (genetic algorithm, contour deformation, and Davidon–Fletcher–Powell) to assess the usefulness of these methodologies for designing optimized nonaxisymmetric liners. This assessment is performed using a multimodal noise source in a finite length rectangular duct without flow. The sparse solver is found to reduce memory requirements by a factor of 5 and processing time by a factor of 11 when compared with the commonly used solver. All three optimization techniques give nearly the same optimum impedance for uniform liners, and this impedance approaches the Cremer optimum impedance at low frequency where only the plane wave mode is cuton. For nonaxisymmetric liners, the genetic algorithm gives improvements in optimum attenuation over the other optimization methodologies because of the presence of multiple local optima. Another important result is the discovery that, when optimized, a spanwise segmented liner with two segments gives attenuations equal to or substantially greater than an optimized axially segmented liner with the same number of segments.

Nomenclature

$[A]$	=	system matrix
A_{qm}	=	rigid-wall duct mode coefficients, Pa
$\{B\}$	=	vector of source effects, Pa
c_0	=	sound speed in duct, m/s
E	=	axial acoustic intensity, Pa m/s
F	=	noise suppression, dB
f	=	source frequency, Hz
H, W, L	=	height, width, and length of duct, m
i	=	$\sqrt{-1}$
k	=	freespace wave number, (ω/c_0), m^{-1}
NX	=	number of transverse grid points
NY	=	number of spanwise grid points
NZ	=	number of axial grid points
p	=	time-independent acoustic pressure, Pa
R, χ	=	normalized acoustic resistance and reactance
Re{ }	=	real part of complex expression
t	=	dimensional time, s
x, y, z	=	transverse, spanwise, and axial coordinate, m
$\partial p/\partial n$	=	normal derivative of acoustic pressure at a boundary surface, Pa/m
ζ	=	normalized acoustic impedance, $R + i\chi$
ρ_0	=	ambient density, kg/m^3
$\{\Phi\}$	=	vector of unknown node pressures, Pa
ω	=	angular frequency, $2\pi f$, s^{-1}
∇^2	=	three-dimensional Laplace operator, m^{-2}

Subscripts

e, s	=	exit and source plane
I	=	Ith impedance segment
N, M	=	upper indices of summation
opt	=	Cremer[25,26] optimum impedance
q, m	=	lower indices of summation

Superscript

$*$	=	complex conjugate

I. Introduction

THE current fleet of large commercial aircraft has successfully achieved Federal Aviation Administration (FAA) noise certifications due, in part, to successful application of passive duct liner treatments to control engine noise. One of the goals of NASA is to develop technologies to improve the sound-absorbing properties of these treatments so that they remain effective in modern, low-drag producing, wide-chord-fan engines.[1] Figure 1 shows axisymmetric and nonaxisymmetric passive duct liner concepts that have potential application to this class of engines. Initially, liner research was limited to uniform liners installed in the engine ducts of the current aircraft fleet. Lansing and Zorumski[2] found that liners could be made more effective by taking advantage of acoustic impedance changes in axial segments. Consequently, the axially segmented liner was studied extensively by several investigators in the 1970s.[3–8] However, the axially segmented lining configuration was not implemented in modern aircraft engines because their optimum design requires an accurate description of the modal distribution of acoustic energy in the sound source. The problem of determining the modal amplitude and phasing of source modes within wide-chord-fan engine ducts is extremely difficult. However, there has been recent progress in determining these quantities.[9]

In the nonaxisymmetric liner concepts (Fig. 1), the duct length is less important because the segmentation is around the circumference instead of along the axis. A beneficial effect of the circumferentially segmented liner configuration was first observed in the mid-1970s by Mani,[10] who simply hardened segments of a uniform liner with strips of aluminum tape. Improved acoustic performance of this configuration was ascribed to mode reconditioning, that is, mode scattering. Several studies,[11–14] all based on modal analysis, have followed the experiment of Mani. However, the potential of optimized, circumferentially segmented liners has never been fully

Received 24 April 2002; revision received 6 February 2004; accepted for publication 5 March 2004.

*Senior Research Scientist, Computational Modeling and Simulation Branch, Mail Stop 128; Willie.R.Watson@NASA.gov. Senior Member AIAA.

†Research Scientist, Structural Acoustics Branch, Mail Stop 463; Michael.G.Jones@NASA.gov. Member AIAA.

‡Senior Research Scientist, Structural Acoustics Branch, Mail Stop 463; Tony.L.Parrott@NASA.gov.

§Senior Research Scientist, Analytical and Computational Structures Branch, Mail Stop 240; Jaroslaw.Sobieski-1@NASA.gov. Fellow AIAA.

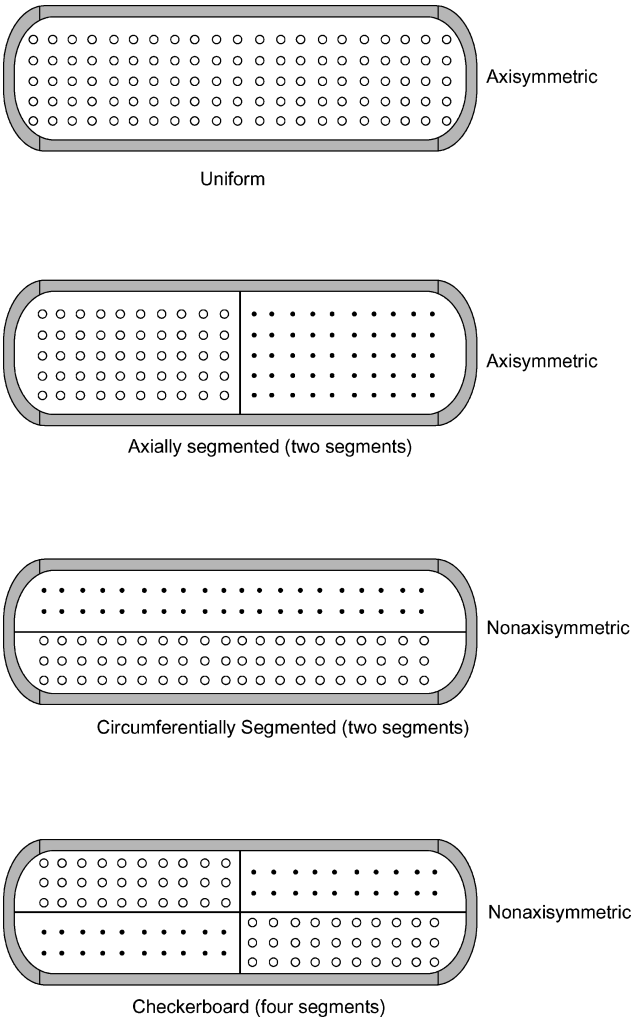

Fig. 1 Passive liner impedance concepts.

evaluated because the modal analysis techniques have been based on the attenuation of a single mode.

The potential synergy between axial and circumferential segmentation can be implemented by the checkerboard liner (Fig. 1). To date, no experimental or analytical studies of this liner configuration have been reported. This is at least partially because the checkerboard liner is not amenable to multimodal analysis techniques. The checkerboard liner configuration requires the use of a fully three-dimensional analysis code for accurate modeling. However, three-dimensional aeroacoustic analysis codes are not yet available because of the excessive computational time and memory requirements of the most commonly used equation solvers. It is interesting that although major advances in equation solving methodologies have occurred during the past decade, these advances have yet to be implemented into major aeroacoustic analysis codes.

The work presented in this paper was motivated by the need to implement more efficient equation solvers and improved optimizers into aeroacoustic liner design codes and by the need for more effective passive liner treatments for the next generation of aircraft engines. In this paper, computation times and memory requirements for a commonly used solver are compared with those of a state-of-the-art, parallel, sparse solver. The sparse solver is used in conjunction with three optimization algorithms to perform liner optimization studies in a rectangular duct without flow. The integrity of each algorithm is evaluated by comparing results obtained from each optimization methodology. We perform an initial assessment of the nonaxisymmetric liner concept by comparing its optimum noise attenuation to those of optimized uniform and axially segmented liners. This assessment is performed with a specific duct geometry and for two source frequencies (4.0 and 7.0 kHz). All cuton

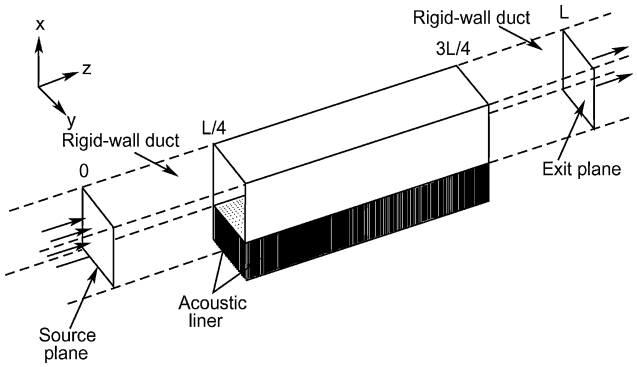

Fig. 2 Three-dimensional duct and coordinate system.

modes are included in the sound source definition, and the analysis uses a geometry and duct termination corresponding to that of the grazing incidence tube in the NASA Langley Research Center Flow Impedance Test Facility. This geometry and termination were selected to allow convenient experimental corroboration at a later date.

II. Statement of Problem

Figure 2 is a schematic of the three-dimensional duct and right-handed coordinate system used to model the grazing incidence tube (GIT). Although the GIT provides for mean flow, it was set to zero for this study because the physical duct termination of the GIT (located downstream of the exit plane) is in its most nonreflective state relative to plane acoustic waves in zero flow. Thus, the exit boundary condition could be better established in zero flow. A second reason for not including flow effects is to reduce the number of optimization studies. The introduction of flow would require that an optimization study be performed at each flow Mach number. The 40.64-cm-long liner is axially centered in the test section (the section of the duct between the source and exit plane), and the upper wall and two sidewalls of the test section are rigid (Fig. 2). Strictly speaking, the rectangular geometry of the GIT does not permit a study of circumferentially segmented liners. However, we will allow the liner impedance to be segmented in the spanwise direction (y direction) of the GIT. This will cause scattering of acoustic energy into spanwise modes, thus, simulating the effects of circumferential segmentation in a circular geometry. Acoustic waves will be propagated from left to right across the surface of the liner and into the termination section of duct. The test section is 81.28 cm in length and has a 5.08×5.08 cm^2 cross section. The source and exit planes are located in rigid-wall sections of duct that are 20.32 cm in length. Note that the exit plane impedance and the liner surface acoustic impedance are generally functions of position. Throughout this paper all impedances are normalized with respect to the characteristic impedance, $\rho_0 c_0$, of the air in the duct. The problem at hand is to determine the liner acoustic impedance that maximizes the noise attenuated by each of the lining concepts.

III. Governing Equations

The mathematical problem is to find the solution to the Helmholtz equation (see Ref. 15)

$$\nabla^2 p + k^2 p = 0 \tag{1}$$

where a time convention of the form $e^{i\omega t}$ is assumed. The boundary condition along the rigid-wall portions of the duct is equivalent to the requirement that the gradient of acoustic pressure normal to the wall vanishes, that is,

$$\frac{\partial p}{\partial n} = 0 \tag{2}$$

At the duct exit, $z = L$, a variety of boundary conditions that render the boundary-value problem well posed could be implemented. Often the desired exit boundary condition is the natural boundary

condition for the Helmholtz equation, that is, $\partial p/\partial n$. Specifying the natural boundary condition at the termination of the GIT requires knowledge of the amplitude and phase of each mode that is incident upon the exit plane. However, it is not possible to know these quantities a priori. An alternative to implementing the natural boundary condition at the exit of the duct is to use a nonreflecting boundary condition. Physically, implementing a nonreflecting boundary condition at the exit plane in the GIT is equivalent to attaching an infinite length of lined duct downstream of the exit boundary. The physical termination in the GIT was designed to mimic the characteristic impedance for outgoing plane waves in a hard wall duct with zero flow, that is,

$$\frac{\partial p}{\partial n} = \frac{-ikp}{\zeta_e} \tag{3}$$

where the dimensionless exit impedance is chosen as unity, $\zeta_e = 1$, to simulate an outgoing plane wave. Note that Eq. (3) may not mimic the physical termination of the GIT at frequencies for which higher-order modes are present at the duct termination because the equation may not allow higher-order modes to transmit through the boundary properly. A more rigorous treatment of the exit boundary condition was not carried out because the amplitude and phase of higher-order modes impinging on the exit boundary was not known a priori. However, in a previous study, the use of this boundary condition [Eq. (3)] led to good comparisons with measured data in the GIT.[16]

The wall lining is assumed to be locally reacting, so that the liner boundary condition is[17]

$$\frac{\partial p}{\partial n} = \frac{ikp}{\zeta} \tag{4}$$

At the source plane, $z = 0$, of the duct, the sound source pressure p_s is known. Therefore, the sound source boundary condition is

$$p = p_s \tag{5}$$

In general, the sound source affect both the optimum liner impedance and the amount of sound attenuated by the lining. For this paper, a modal pressure distribution appropriate for a multimodal noise source located in a rigid-wall section of duct

$$p_s = \sum_{q=0}^{N}\sum_{m=0}^{M} A_{qm}\cos\left(\frac{q\pi y}{W}\right)\cos\left(\frac{m\pi x}{H}\right) \tag{6}$$

is used. We assume that cutoff modes have zero amplitudes, $A_{qm} = 0$. The phases of cuton modes are taken as zero, and their amplitudes are determined such that they all have either equal mode amplitudes,

$$|A_{qm}| = |A_{00}| \tag{7}$$

or equal power per mode as determined by the following condition:

$$\frac{\sqrt{k^2 - (q\pi/W)^2 - (m\pi/H)^2}}{kHW|A_{00}|^2}|A_{qm}|^2 \times \int_0^H \int_0^W \cos^2\left(\frac{q\pi y}{W}\right)\cos^2\left(\frac{m\pi x}{H}\right) \mathrm{d}y\,\mathrm{d}x = 1 \tag{8}$$

Others have found that both of these sources are attenuated nearly equally by the liner.[1] Equations (6–8) imply that the sound source does not vary with the introduction of the liner. It will be shown later that this assumption is a valid approximation for the current duct geometry and source.

Equations (1–6) form a well-posed boundary-value problem that can be solved to determine uniquely the acoustic pressure field in the duct. An exact analytical solution for this field is not available for a general input data set; therefore, a numerical method is needed to obtain the solution for this field.

IV. Numerical Solution for Acoustic Pressure

The numerical method used to obtain the solution for the acoustic pressure field is described elsewhere.[18] Only the details necessary for clarity and continuity are presented herein. The solution to Eqs. (1–6) is obtained with a conventional Galerkin finite element method using a brick element and linear basis functions. This methodology results in a large, linear, sparse, and symmetric system of complex equations of the form

$$[A]\{\Phi\} = \{B\} \tag{9}$$

Note that an alternate formulation for the current problem is to specify only the incident pressure wave at the source plane and a nonreflecting boundary condition at the exit plane of the duct. The alternate formulation has the advantage that reflected modes in the hard-wall section on the source end would develop as part of the solution. Thus, it would not be necessary to assume that installing the lining has no effects on the sound source. However, this alternate formulation has the disadvantage that it leads to an unsymmetric matrix $[A]$. The solution to an unsymmetric matrix equation requires twice the CPU time and RAM on a digital computer than a symmetric formulation. This increase would be particularly troublesome because the symmetric formulation already severely taxes computer resources. Additionally, incident pressure is not directly measurable with the single array of microphones currently installed in the GIT. Thus, if the incident pressure were used as the source boundary condition, our plan to compare calculated and measured attenuation would require installation of a second array of microphones to separate the incident and reflected waves with all of the attendant measurement error implied by such a procedure. Finally, the disadvantages of implementing a nonreflecting boundary condition at the exit plane in the GIT have been addressed in the preceding section.

To solve Eq. (9), a parallel, direct, sparse solver factorizes $[A]$ and then obtains the solution vector using the sequential operations of backward and forward substitution. The solver employs a compressed column storage scheme to reduce storage overhead. Only the nonzero coefficients in the upper triangular part of $[A]$ are stored, along with two pointer arrays that store the column numbers and starting indexes of these nonzero coefficients. To obtain the speed necessary for efficient three-dimensional solutions, the sparse solver uses two accelerators: equation reordering[19,20] to reduce fill during the factorization of $[A]$ and parallelization. (The equation solver runs on multiple processors simultaneously.)

The sparse solver initially selected to solve Eq. (9) was a complex version of the Vectored Sparse Solver (VSS).[21] This software package is a commercial version of the NASA-developed general-purpose solver[22] that was modified for complex arithmetic and commercialized by the Solversoft Corporation in 1999. However, since that time Silicon Graphics, Inc. (SGI), has developed a parallel sparse solver (ZPSLDLT) that is contained in version 1.4 of the SGI/Cray Scientific Library. Studies performed by the authors show that the complex version of VSS and ZPSLDLT have nearly identical time and memory requirements. In addition, ZPSLDLT is readily available to the public, whereas VSS is proprietary. Consequently, this paper uses ZPSLDLT to solve Eq. (9).

V. Objective Function

The four liner configurations discussed in this paper are restricted to a rectangular geometry of overall dimensions L by W, as shown in Fig. 3. Apart from the uniform liner impedance (baseline), the surface impedance is segmented (Fig. 3) into two or four segments. Each liner impedance segment may default to the baseline uniform liner during liner optimization. However, one segmented liner may not default to another, that is, the checkerboard liner cannot default to the spanwise segmented liner, etc. The goal is to determine the optimum acoustic impedance of each liner segment that maximizes the noise attenuated by the liner. The authors use the reduction in the sound power from the source to the exit of the duct, F, as an objective function that is maximized to determine the optimal attenuation of the liner. This objective function is a real, positive function, has units

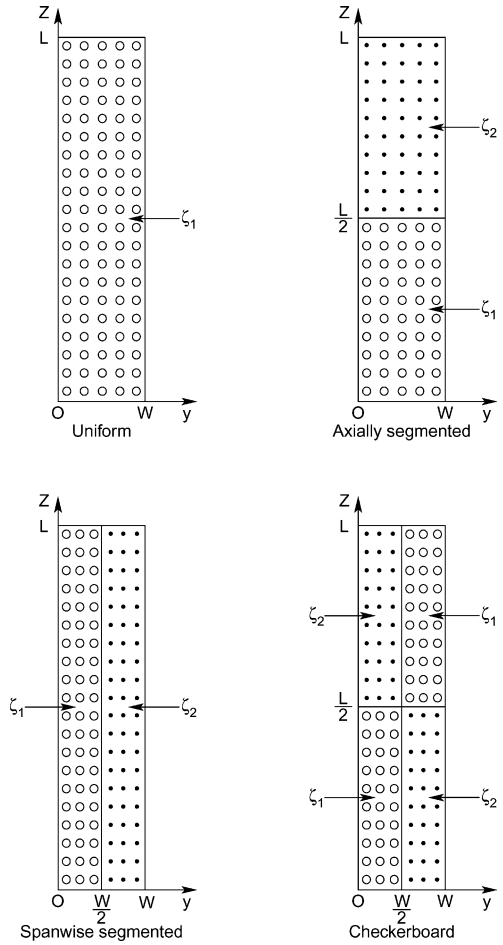

Fig. 3 Schematic of rectangular duct liner configurations.

of decibels, and is defined as[15]

$$F = 10\log_{10}\left[\frac{Re\left\{\int_0^W\int_0^H E(x,y,0)\,dx\,dy\right\}}{Re\left\{\int_0^W\int_0^H E(x,y,L)\,dx\,dy\right\}}\right] \tag{10}$$

$$E(x,y,z) = \frac{ip(x,y,z)}{\rho_0\omega}\frac{\partial p^*(x,y,z)}{\partial z} \tag{11}$$

Because the acoustic pressure field p is known only at a discrete number of points in the duct, the integration in Eq. (10) is performed numerically using Simpson's rule for numerical integration.

VI. Optimization Methods

We use the attenuation F produced by the liner as an objective function and determine the optimum acoustic impedance for each liner segment. For the uniform liner, two parameters are free to vary in the optimization: the acoustic resistance R_1 and reactance χ_1. Thus, contours of constant attenuation [referred to here as a contour map (CM)] will be plotted in the impedance plane to determine the global optimum point for the uniform liner. The segmented liners (Fig. 3) have four parameters to vary: the acoustic resistances R_1 and R_2 and the acoustic reactances χ_1 and χ_2. We used an iterative two-step procedure to determine the optimum point of the segmented liners. The iterative procedure is as follows:

1) Hold the acoustic impedance of the first section ζ_1 equal to that of the optimum uniform liner and use a CM to obtain an optimum ζ_2.

2) Hold ζ_2 at the optimum from step 1 and use a CM to obtain a new optimum ζ_1.

The preceding two-step iterative procedure is repeated until the attenuation of the segmented liner converges within some specified tolerance. This optimization method is referred to herein as the iterative contour deformation method (ICDM). A similar procedure to that used here was used to design an axially segmented liner.[8] Note that as used here the ICDM is not automated because each iteration is guided by hand, using results obtained from a CM.

The optimal point for each segmented liner is also obtained using two automated optimization algorithms. The first automated optimization algorithm was a Davidon–Fletcher–Powell (DFP) optimization algorithm (see Ref. 23). This algorithm has the disadvantages of requiring both an initial starting location and a central difference approximation for the gradient of the objective function. Additionally, the method is known to converge to local optima. The second automated optimization algorithm is a genetic algorithm (GA). The GA initializes a random sample of individuals with different parameters to be optimized using evolution via survival of the fittest. In contrast to the DFP, the GA does not require calculation of the gradient of the objective function, nor does it require an initial starting location. Furthermore, when compared with the DFP, the GA increases the probability of obtaining a global optimum point but at the expense of a significant increase in computational time. A full description of these two automated optimization algorithms is beyond the scope of this paper. Readers who are unfamiliar with the DFP and GA algorithms are encouraged to consult Refs. 23 and 24.

VII. Results and Discussion

Results in this section are presented with the following three objectives in mind: 1) to demonstrate the efficiency of the sparse solver compared to the most commonly used solver, 2) to test the integrity of the optimization methodologies, and 3) to assess the relative merits of the nonaxisymmetric liner concept for the current duct geometry and sound source. The accuracy of the sparse solver has been presented in a previous paper[18] and is not addressed further in this work. All results presented in this paper were computed on an SGI ORIGIN 2000 computer platform using double-precision (64-bit) arithmetic.

A. Solver Efficiency Studies

Table 1 shows the minimum number of points required to resolve all cuton modes (assuming 12 points per wavelength) in the rigid-wall duct for frequencies up to 21.0 kHz. Here, *NX*, *NY*, and *NZ* are the minimum number of equally spaced points in the x, y, and z directions, respectively, to resolve all cuton modes. The current industry practice is to use scale models as small as one-fifth the size of full-scale engines in liner designs. The largest full-scale frequency of interest is typically 4.0 kHz. Thus, the largest frequency of interest for the smallest scale (a one-fifth-scale model) is 20.0 kHz. To fully capture this frequency range, the results in Table 1 are given up to a frequency of 21.0 kHz. Note that at the highest frequency (21.0 kHz) a matrix order of 776,304 is required to resolve accurately all cuton modes. Typically, band solvers have been the solver of choice for obtaining the solution to the indefinite, linear system given by Eq. (9). However, it will be shown that band solvers are too expensive for optimization studies in three spatial dimensions and newer more efficient equation solving methodologies are needed. To understand better the improvement in efficiency of equation solving methods over the past decade, it is helpful to compare the CPU time and RAM required to obtain the solution to Eq. (9) using a commonly

Table 1 Minimum points for resolving cuton modes

f, kHz	*NX*	*NY*	*NZ*	$NX \times NY \times NZ$
4.0	6	6	114	4,104
7.0	12	12	200	28,800
11.0	18	18	313	101,412
14.0	24	24	399	229,824
17.0	30	30	484	435,600
21.0	36	36	599	776,304

used band solver to that of the sparse solver (ZPSLDLT) used in this paper.

The CPU time and RAM for the band and sparse solvers are shown in Fig. 4. Results are presented using a dual-axis system with the CPU time and RAM referenced to the $Y1$ and $Y2$ axes, respectively. CPU times are given in kiloseconds, and the RAM requirements are given in gigabytes. Results in Fig. 4 were computed on a single processor and without equation reordering. As shown in Fig. 4 at higher frequencies, the sparse solver consumes 20% less CPU time (2 h less) and only half the RAM of the band solver. Typically, optimizers require thousands of function evaluations, that is, passes through the solver, to obtain an optimum point. Without further increases in processing speed, it will be impractical to perform optimization studies even with the more efficient sparse solver at the higher frequencies.

The sparse solver has been accelerated with equation reordering to minimize fill during matrix factorization. Figure 5 shows the additional reduction in CPU time that can be obtained using multiple minimum degree (MMD) reordering[19] and nested dissection (ND) reordering[20] on a single processor. The savings in CPU time at the higher frequencies due to equation reordering are clearly evident. Relative to the CPU time without reordering, MMD reordering reduces the CPU time by 14%, whereas a reduction of nearly 64% is

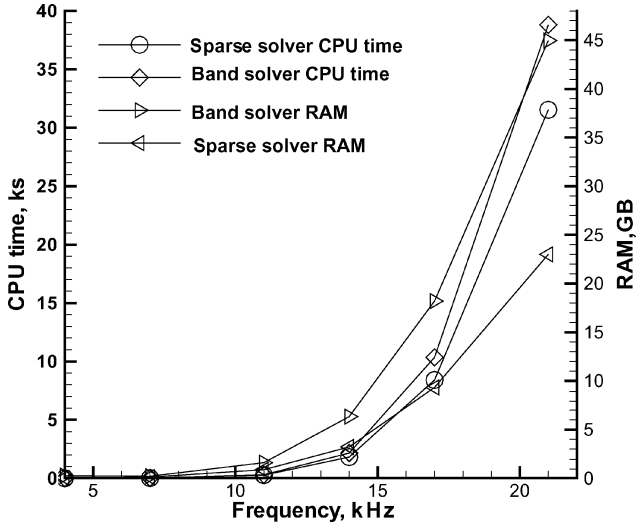

Fig. 4 Single-processor CPU times and RAM requirements for band and sparse solvers.

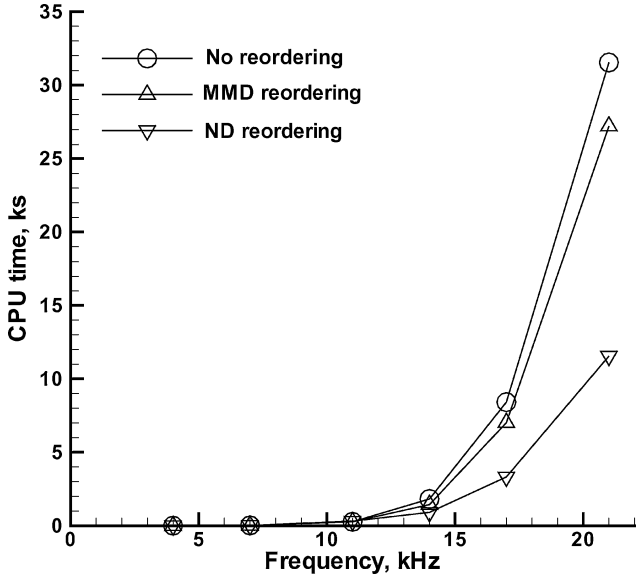

Fig. 5 Effects of equation reordering on CPU times of sparse solver.

Table 2 Sparse solver parallel speedup at 14.0 kHz

Number of processors	Parallel speedup
2	1.79
4	3.15
8	4.60
16	5.80

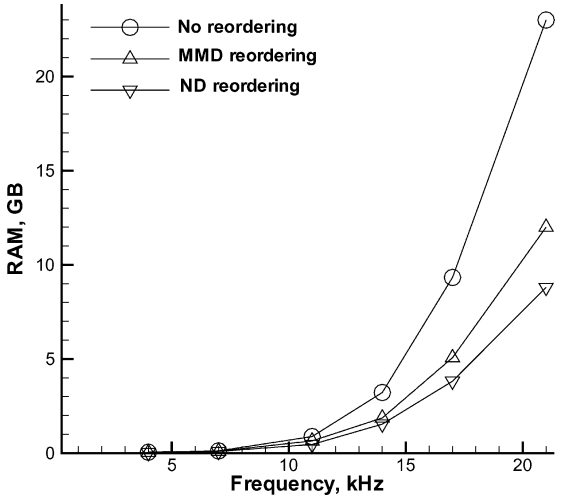

Fig. 6 Effects of equation reordering on RAM requirements of sparse solver.

achieved with ND reordering. Results in Fig. 6 show how the reordering schemes reduce the RAM requirements of the sparse solver. Relative to the RAM requirements without reordering, note that at higher frequencies MMD and ND reordering reduces the RAM requirements of the solver by factors of two and three, respectively. Thus, compared with the band solver, the sparse solver with ND reordering reduces the CPU time and RAM requirements by factors of 3.4 and 2.6, respectively, at the higher frequencies.

A second method for reducing the CPU time of the sparse solver is parallelization. Table 2 gives a comparison of the parallel speedup obtained at a frequency of 14.0 kHz when the solver is run on 2, 4, 8, and 16 processors. The reference timing for computing the parallel speedup is that required for a solution using the parallel version of the sparse solver on a single processor. The solver is observed to run efficiently on up to four processors. Note that the speedup is 1.79 and 3.15 on two and four processors, respectively. There is only a modest improvement in parallel speedup for more than four processors. Furthermore, the sparse solver running on only four processors with ND reordering reduces the CPU time by a factor of nearly 11 when compared with that of the more commonly used band solver (Fig. 4).

B. Optimization Studies

The uniform, axially segmented, spanwise segmented, and checkerboard liners are optimized at two source frequencies, 4.0 and 7.0 kHz. At 4.0 kHz, the sound source contains three cuton modes [the (0, 0), (1, 0), and (0, 1) modes], whereas at 7.0 kHz the sound source contains six cuton modes [the (0, 0), (1, 0), (0, 1), (1, 1), (2, 0), and (0, 2) modes]. Based on the efficiency studies of the preceding section, it was decided to run the sparse solver in parallel on four processors using ND reordering. The initial liner design used a spatial grid that was designed to capture all cuton modes in a rigid-wall duct for the 7.0-kHz sound source ($NX = NY = 13$ and $NZ = 201$). After the optimum liner was determined, a grid refinement study was conducted, and it was determined that this spatial grid could accurately resolve the attenuation at the optimum point.

Uniform Liner

Figures 7 and 8 show a contour map of the uniform liner attenuation function at 4.0 and 7.0 kHz, with evenly spaced grids

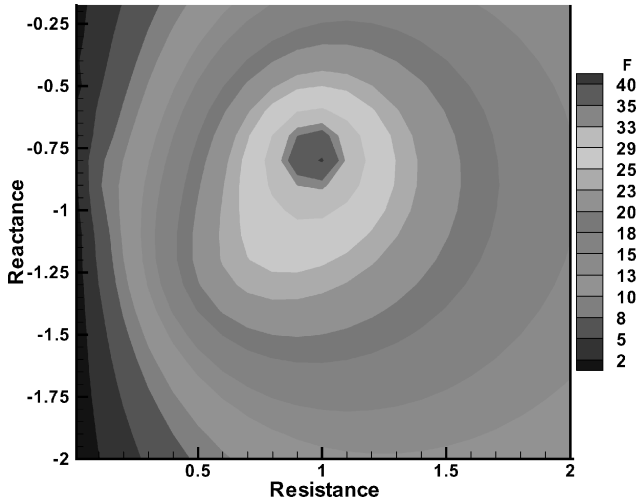

Fig. 7 Uniform liner contour map for 4.0-kHz source.

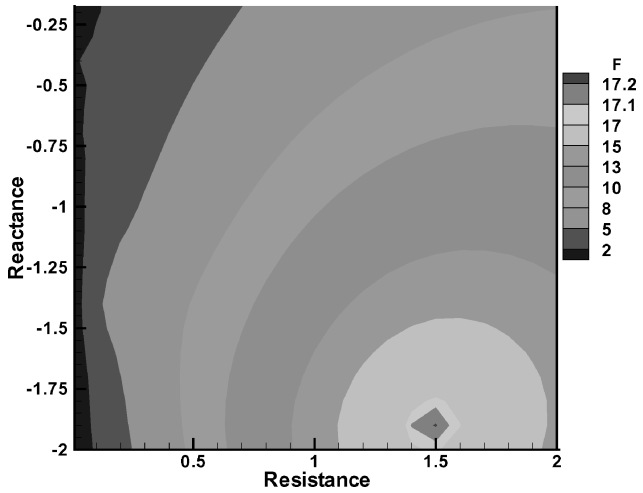

Fig. 8 Uniform liner contour map for 7.0-kHz source.

of 100 and 200 points along the resistance and reactance axes, respectively. Here we have used the equal mode amplitude source. Note that the attenuation function has a single, well-defined optimum point at each frequency: $\zeta = 1.05 - 0.80i$ and $F = 41.0$ dB at 4.0 kHz and $\zeta = 1.48 - 2.0i$ and $F = 17.2$ dB at 7.0 kHz. The DFP and GA algorithms were also used to obtain the optimum point of the uniform liner with the equal mode amplitude source. The DFP algorithm was initialized from the following four starting locations in the impedance plane:

$$\zeta_1 = 2.5 - 5.0i, \qquad \zeta_1 = 2.5 + 5.0i$$

$$\zeta_1 = 7.5 - 5.0i, \qquad \zeta_1 = 7.5 + 5.0i \tag{12}$$

The optimum points obtained with the DFP for each of these starting locations were nearly identical. Generally, the DFP converged to the optimum point in four to eight iterations (depending on the starting location) and each iteration required approximately 4 min of CPU time. Note that the GA results were computed using a population size of 40 and were observed to converge in 40–50 generations.

Because each optimization algorithm gives nearly the same design points for the uniform liner, it is of interest to compare the relative efficiency of each algorithm. The CM uses a relatively fine grid (100×200 grid) in the design space so that 20,000 function evaluations (equation solves) are needed for the CM method. In the DFP algorithm, the gradient of the objective function is computed numerically by using a central difference formula. Thus, five function evaluations are required per DFP iteration. On the other hand, the GA uses a population density of 40 (40 equation solves per generation). Thus, a single GA generation requires approximately the same computer memory and CPU time as eight DFP iterations. Therefore, 20,000, 2000, and 200 function evaluations were used to compute optimization results for the CM, GA, and DFP, respectively.

Table 3 Uniform liner results

f, kHz	R_1	χ_1	F, dB
	DFP		
4.0	0.96	−0.78	45.80
7.0	1.47	−1.91	17.20
	GA		
4.0	0.97	−0.77	45.60
7.0	1.48	−1.90	17.20
	CM		
4.0	0.98	−0.80	40.50
7.0	1.45	−1.90	17.10

Clearly, the CM is considerably more expensive than the other optimization algorithms because it contains many more function evaluations. The CM, therefore, contains considerably more information about off-design performance than the GA, and the GA contains considerably more information about this parameter than the DFP. Note also that although the DFP uses only 1/10th the CPU time used by GA, it is generally less reliable than the GA because it is more likely to converge to a local optimum. The existence of multiple local optima is particularly problematic for segmented liner design studies, as will be demonstrated in the next section.

The uniform liner optimum points achieved with the DFP, GA, and CM (using the equal mode amplitude source) are given in Table 3. As noted earlier, each optimization methodology converged to nearly the same impedance at each frequency, and the optimum attenuations are nearly identical at 7.0 kHz. However, at 4.0 kHz, the DFP and GA optimum attenuations differ from the CM result by approximately 5 dB (nearly 10%). A refinement of the impedance grid about the CM optimum point shows that this difference in attenuation reflects the sensitivity of the attenuation to changes in the second and third decimal places of the impedance at the optimum point. This indicates that the impedance grid used to construct the CM was not fine enough to determine the optimum attenuation with greater accuracy at the optimum point. Such sensitivities are known to exist at other points in the impedance space, that is, local optima of multisegmented liners or at resonance and antiresonance.

Note that the maximum attenuation is significantly reduced when the frequency is increased from 4.0 to 7.0 kHz (Table 3). The ineffectiveness of the uniform liner at the higher frequencies is the primary reason for investigating the segmented lining concepts. Furthermore, a study of the contour plot tabular data (available from the authors by request) shows that, away from the optimum point, the greatest attenuation occurs at resonance, $\chi = 0.0$. However, for finite values of acoustic reactance (and away from the optimum point) the largest attenuation is obtained when the acoustic resistance and reactance have equal magnitude but are opposite in sign.

At the lowest frequency (4.0 kHz),the optimum acoustic impedance obtained from each of the uniform liner optimization methods (Table 3) is nearly identical to the Cremer[25] optimum acoustic impedance (see Ref. 26) for the lowest-order mode (LOM) in the infinite duct:

$$\zeta_{\text{opt}} = (0.929 - 0.744i)(kH/\pi) \tag{13}$$

This is what one would expect at low frequencies where higher-order modes in the hard-walled sections are cutoff and most of the energy is carried in the plane wave mode. Note that considerable differences exist between the Cremer optimum and the current results at the highest frequency (7.0 kHz). These results confirm that, even for the multimodal source at low frequency, the optimum acoustic impedance in a finite length duct (at least for $L/H = 8$) is still dominated by the least attenuated mode, whose attenuation will be maximized by the Cremer optimum acoustic impedance for

the LOM. The fact that the current methods reproduce the Cremer optimum acoustic impedance at low frequency and deviate from it at the higher frequency gives further credence to the methodologies used in this paper.

One contentious issue that has not been addressed is the effect on the optimum point of the hard-wall section of duct on the source end. The phase of incident modes in the hard-wall sections of duct are generally affected by the length of this hard-wall section. To address this question, additional optimization studies were conducted with an equal mode amplitude source without a spanwise source distribution, that is, $A_{qm} = 0$, for $q \neq 0$. This source greatly reduces the computational time and memory required to obtain the optimum point because the duct can be modeled as a two-dimensional problem in the (x, z) plane. However, this two-dimensional model still adequately represents the effects of the hard-wall lengths with reasonable physical fidelity. Optimization results were computed with the hard wall length ranging from $\frac{1}{2}$ to 16 duct heights. The height of the duct H, lining length, $8H$, and hard-wall length on the exit end of the duct, $4H$, were fixed to that of the GIT. As the hard-wall length upstream of the liner was varied, the computational grid along the axial direction of the duct was varied to maintain an axial resolution of 12 points per wavelength.

Optimization results obtained from the GA algorithm that show the effects of the hard-wall length at 4.0 and 7.0 kHz are presented in Table 4. When the hard-wall length is greater than two duct heights, $2H$, there is little effect on the optimum attenuation. As the hard-wall length is reduced below two duct heights, the effects of the hard-wall length become more noticeable. Generally speaking, the effect of the hard-wall length is greatest at the highest frequency, 7.0 kHz, and there is a greater spread in the optimum resistance. The GIT that is modeled in this work has a hard-wall length of four duct heights, $4H$. Based on the results of this study, this hard-wall length will have minimal impact on the optimum attenuation produced by the wall lining. A computational study also showed only minimal changes in the optimum point when either an equal mode amplitude or equal power per mode source was used. The optimal points obtained for both sources are presented in Table 5. In the evaluation of source effects, the duct was modeled as a two-dimensional problem in the (x, z) plane just as in the hard-wall length study.

Segmented Liners

The ICDM, DFP, and GA algorithms have been used with the segmented liners in an attempt to obtain optimum attenuations greater than that of an optimum uniform liner. All results reported in this section were obtained by using the equal mode amplitude source (with relative phases set to zero). The ICDM was not successful when used with the segmented liners. It was discovered that the ICDM converged to the uniform liner optimum. The failure of the ICDM to converge to an optimum point different than the uniform liner is contrary to the results of Ref. 8. However, note that the duct geometry, source, and frequency used in this study are significantly different from those used in Ref. 8. These results suggest that the success or failure of ICDM is dependent on liner construction (uniform, axially segmented, or circumferentially segmented), source structure, frequency content, or duct geometry. Thus, only the DFP and GA optimization results are presented for the segmented liners. Furthermore, in the segmented lining design studies, the DFP was initiated from the 16 different starting locations given in Table 6. As expected, it was found that the segmented liner attenuation function contains multiple local optima. Thus, the DFP results were extremely sensitive to the starting locations and were, therefore, less reliable than the GA. The DFP optimum presented in this section corresponds, therefore, to the local optimum with the largest attenuation out of the 16 starting locations. Table 7 shows a comparison of the optimum attenuations obtained from the DFP and GA algorithm for the checkerboard liner. Observe that both the DFP and GA returned the optimum uniform liner design point for the checkerboard liner. Tables 8 shows a comparison of the optimum points obtained with the DFP and GA for the axially segmented liner. For this liner, both optimization methodologies give nearly the same optimum attenuation, but the optimum impedances predicted (from each method) for the first and second segments are distinctly different. Optimization results for the spanwise segmented liner are given in Table 9. Note that, for this liner, the two optimization methodologies show significant differences in both the optimum attenuation and the impedance of the second segment at 4.0 kHz. On the other hand, for the 7.0 kHz source, there is only a modest difference in the attenuation and impedances at the optimum point.

Table 4 Effects of hard-wall length on optimum attenuation

Hard-wall length	R_1	χ_1	F, dB
	4.0 kHz		
$16H$	1.18	−1.06	40.5
$8H$	1.10	−1.06	41.1
$4H$	1.10	−1.06	41.4
$2H$	1.10	−1.06	41.1
H	1.18	−1.06	39.6
$H/2$	1.10	−1.06	42.5
	7.0 kHz		
$16H$	1.02	−2.24	17.0
$8H$	1.02	−2.24	17.4
$4H$	2.28	−2.39	17.1
$2H$	2.13	−2.47	12.5
H	1.42	−2.39	13.4
$H/2$	1.81	−2.31	14.8

Table 5 Optimal attenuation for equal mode amplitude source and equal power per mode source

f, kHz	R_1	χ_1	F, dB
	Equal mode amplitude		
4.0	0.787	−0.902	46.4
7.0	0.945	−2.000	22.6
	Equal power per mode source		
4.0	0.787	−0.902	46.0
7.0	1.181	−2.157	22.51

Table 6 Starting locations for DFP

Location	ζ_1	ζ_2
1	$2.5-5.0i$	$2.5-5.0i$
2	$2.5-5.0i$	$2.5+5.0i$
3	$2.5-5.0i$	$7.5-5.0i$
4	$2.5-5.0i$	$7.5+5.0i$
5	$2.5+5.0i$	$2.5-5.0i$
6	$2.5+5.0i$	$2.5+5.0i$
7	$2.5+5.0i$	$7.5-5.0i$
8	$2.5+5.0i$	$7.5+5.0i$
9	$7.5-5.0i$	$2.5-5.0i$
10	$7.5-5.0i$	$2.5+5.0i$
11	$7.5-5.0i$	$7.5-5.0i$
12	$7.5-5.0i$	$7.5+5.0i$
13	$7.5+5.0i$	$2.5-5.0i$
14	$7.5+5.0i$	$2.5+5.0i$
15	$7.5+5.0i$	$7.5-5.0i$
16	$7.5+5.0i$	$7.5+5.0i$

Table 7 Checkerboard liner results

f, kHz	R_1	χ_1	R_2	χ_2	F, dB
		DFP			
4.0	0.96	−0.77	0.95	−0.78	45.10
7.0	1.47	−1.90	1.46	−1.91	17.20
		GA			
4.0	0.96	−0.78	0.96	−0.77	45.20
7.0	1.48	−1.91	1.47	−1.90	17.20

Table 8 Axially segmented liner results

f, kHz	R_1	χ_1	R_2	χ_2	F, dB
		DFP			
4.0	0.95	−0.94	0.88	−0.51	48.52
7.0	0.86	−2.29	1.45	−0.70	32.90
		GA			
4.0	0.83	−0.98	1.30	0.03	49.02
7.0	0.91	−2.40	1.30	−0.90	35.60

Table 9 Spanwise segmented liner results

f, kHz	R_1	χ_1	R_2	χ_2	F, dB
		DFP			
4.0	1.00	−0.80	0.93	−0.76	47.02
7.0	0.69	−2.70	0.83	−0.91	27.72
		GA			
4.0	0.91	−0.98	0.76	−0.28	58.80
7.0	0.91	−2.47	1.14	−0.90	31.54

The most significant result to be gleaned from these segmented liner studies is that the axially segmented and spanwise segmented liners give better attenuation than the uniform liner (Table 3). At 4.0 kHz, the optimized axially and spanwise segmented liners give 3.0 and 14.0 dB, respectively, of additional attenuation compared with that of the optimized uniform liner. The spanwise segmented liner is clearly a better attenuator of sound than the axially segmented liner when optimized for a 4.0-kHz multimodal source. At 7.0 kHz, the segmented liner designs have nearly the same attenuation but distinct acoustic impedance values. Furthermore, at 7.0 kHz, the segmented liner attenuations are nearly double that of the uniform liner. In general, the DFP optimum design point gives less attenuation than the GA design point for the segmented liners (Table 8).

VIII. Conclusions

Based on the results of this study, the following conclusions are drawn:

1) The sparse solver (running in parallel on four processors with ND reordering) reduces CPU time and RAM requirements by factors of 11 and 5, respectively, when compared with the commonly used band solver.

2) Even for a multimodal noise source in a finite length duct at low frequency, the optimum uniform liner acoustic impedance is dominated by the least attenuated mode, in which attenuation is maximized by the Cremer optimum acoustic impedance.

3) DFP and GA are useful design tools for the segmented liner, but the success of the ICDM seems dependent on segmented liner construction, source structure, frequency content, or duct geometry.

4) Because segmented liners contain multiple local optima, the GA generally leads to a better design than the DFP algorithm.

5) An optimized spanwise segmented liner is more effective at attenuating sound than an optimized uniform liner. It tends to be more effective at the higher frequencies and gives attenuations equal to or substantially greater than an optimized axially segmented liner.

The nonaxisymmetric liner optimization results are sufficiently encouraging to warrant additional studies. Note that the conclusions of this paper apply only to the source, frequency, and duct geometry for which this study was conducted. Considerable care should be exercised in attempting to generalize these conclusions to other geometries, source structures, and frequencies. Future work is expected to target frequencies in the 8.0–21.0-kHz range. Sample calculations presented (Fig. 5) show that a single function evaluation with the current sparse solver at 21.0 kHz requires nearly an hour of CPU time. When it is assumed that 1000–2000 function evaluations are required to obtain the optimum, the current solver would have to be accelerated nearly two orders of magnitude before optimization studies become practical at the highest frequency. Because it is unlikely that the current sparse solver can be accelerated to this degree, it seems reasonable that a response surface methodology will most likely be required for function evaluations at the higher frequencies. Furthermore, if more segments (with distinct acoustic impedance values) are desired at even moderate frequencies, a response surface methodology will most likely be required. In addition, the designs considered in this paper have been concerned with noise suppression at a single frequency. However, the total performance of a lining configuration must be measured by its off-design performance as well. Future investigations should also be concerned with off-design performance.

Acknowledgment

The authors gratefully acknowledge Jay H. Robinson of the Structural Acoustics Branch at the NASA Langley Research Center for his useful suggestions and assistance with the genetic algorithm.

References

[1]Bielak, G. W., Premo, G. W., and Hersh, A. S., "Advanced Turbofan Duct Liner Concepts," NASA CR-1999-209002, Feb. 1999.

[2]Lansing, D. L., and Zorumski, W. E., "Effects of Wall Admittance Changes on Duct Transmission and Radiation of Sound," *Journal of Sound and Vibration*, Vol. 27, No. 1, 1973, pp. 85–100.

[3]Zorumski, W. E., "Acoustic Theory of Axisymmetric Multisectioned Ducts," NASA TR R-419, June 1974.

[4]Motsinger, R. D., Kraft, R. E., Paas, J. E., and Gahn, B. M., "Analytical and Experimental Results of Some Segmented Liner Acoustic Performance Studies for High Mach Number Inlets," NASA CR-2882, June 1974.

[5]Quinn, D. W., "Attenuation of the Sound Associated with a Plane Wave in a Multisectioned Duct," AIAA Paper 75-496, March 1975.

[6]Sawdy, D. T., Beckmeyer, R. J., and Pattern, J. D., "Optimum Segmented Acoustic Liners for Flow Ducts," 90th Meeting of the Acoustical Society of America, Paper D6, Nov. 1975.

[7]Lester, H. C., and Posey, J. W., "Optimum One-Section and Two-Section Circular Sound Absorbing Duct Liners for Plane-Wave and Monopole Sources Without Flow," NASA TN D-8348, 1976.

[8]Kraft, R. E., "Theory and Measurement of Acoustic Wave Propagation in Multi-Segmented Rectangular Flow Ducts," Ph.D. Dissertation, Dept. of Mechanical Engineering, Univ. of Cincinnati, Cincinnati, OH, June 1976.

[9]Heidelberg, L. J., Rice, E. J., and Homyal, L., "Acoustic Mode Measurement in the Inlet of a Model Turbofan Using a Continuously Rotating Rake," *Journal of Aircraft*, Vol. 32, No. 4, 1995, pp. 761–767.

[10]Mani, R., "Acoustic Duct with Peripherally Segmented Acoustic Treatment," U.S. Patent 3,937,590, Feb. 1976.

[11]Astley, R. J., Walkington, N. J., and Eversman, W., "Transmission in Flow Ducts with Peripherally Varying Linings," AIAA Paper 80-1015, June 1980.

[12]Watson, W. R., "Circumferentially Segmented Duct Liners Optimized for Axisymmetric and Standing-Wave Sources," NASA TP-2075, Sept. 1982.

[13]Watson, W. R., "An Acoustic Evaluation of Circumferentially Segmented Duct Liners," *AIAA Journal*, Vol. 22, No. 9, 1984, pp. 1229–1233.

[14]Parrott, T. L., and Watson, W. R.,"Comparison of Measured and Calculated Mode Redistribution Associated with Spinning Mode Transmission Through Circumferentially Segmented Lined Ducts," NASA TM-84576, March 1983.

[15]Morse, P. M., and Ingard, K. U., *Theoretical Acoustics*, McGraw–Hill, New York, 1968, pp. 495, 496.

[16]Jones, M. G., Parrott, T. L., and Watson, W. R., "Comparison of Acoustic Impedance Eduction Techniques for Locally-Reacting Liners," AIAA Paper 2003-3306, May 2003.

[17]Myers, M. K., "On the Acoustic Boundary Condition in the Presence of Flow," *Journal of Sound and Vibration*, Vol. 71, No. 3, 1980, pp. 429–434.

[18]Watson, W. R., "Three-Dimensional Rectangular Duct Code with Application to Impedance Eduction," *AIAA Journal*, Vol. 40, No. 2, 2002, pp. 217–226.

[19]Liu, J., "Modification of the Minimum-Degree Algorithm by Multiple Elimination," *Association for Computing Machinery, Transaction on Mathematical Software*, Vol. 11, No. 2, 1985, pp. 141–153.

[20]George, A., and Liu, J., *Computer Solution of Large Sparse Positive Definite Systems*, Prentice–Hall, Englewood Cliffs, NJ, 1981, Chaps. 5 and 10.

[21]VSS Sparse Linear Equation Solver, http://Solversoft.Com, 1999.
[22]Storaasli, O. O., "Performance of NASA Equation Solvers on Computational Mechanics Applications," *Proceedings of the 37th AIAA/ASME/ASCE/ANS/ASC Structures, Structural Dynamics, and Materials Conference*, AIAA Reston, VA, 1996, pp. 1680–1685.
[23]Stewart, G. W., III, "A Modification of Davidon's Minimization Method to Accept Difference Approximations of Derivatives," *Journal of Association for Computing Machinery*, Vol. 14, No. 1, 1967, pp. 72–83.
[24]Goldberg, D., *Genetic Algorithms in Search, Optimization and Machine Learning*, Addison–Wesley, New York, 1989, pp. 75–147.
[25]Cremer, L., "Theory of Sound Attenuation in a Rectangular Duct with an Absorbing Wall and the Resultant Maximum Attenuation Coefficient," McDonnell-Douglas Corp., Rept. MCD-J6630, Long Beach, CA, July 1974; translated from *Acoustics*, Vol. 3, No. 2, 1953, pp. 249–263.
[26]Tester, B. J., "The Optimization of Modal Sound Attenuation in Ducts, in the Absence of Mean Flow," *Journal of Sound and Vibration*, Vol. 27, No. 4, 1973, pp. 477–513.

H. M. Atassi
Associate Editor